

# Variable-range electron hopping, conductivity cross-over and space-charge relaxation in C<sub>60</sub>Br<sub>6</sub>

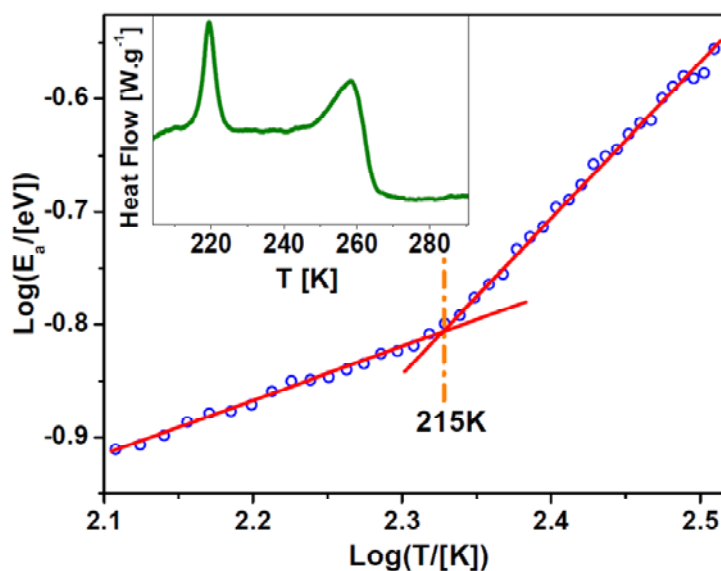
Manesh Zachariah,<sup>1</sup> Michela Romanini,<sup>1</sup> Panagiota Zygouri,<sup>2</sup> Dimitrios Gournis,<sup>2</sup> Josep Lluís Tamarit,<sup>1</sup> Maria Barrio,<sup>1</sup> and Roberto Macovez<sup>1, \*</sup>

<sup>1</sup> Grup de Caracterització de Materials, Universitat Politècnica de Catalunya, Departament de Física, ETSEIB, Av. Diagonal 647, E-08028 Barcelona, Spain

<sup>2</sup> Department of Materials Science and Engineering, University of Ioannina, 45110 Ioannina, Greece

**ABSTRACT.** Dielectric spectroscopy is employed to probe the frequency-dependent conductivity and dipolar dielectric response of solid C<sub>60</sub>Br<sub>6</sub>. Below approximately 215 K, charge conduction is electronic and well described by Mott's variable-range polaron hopping model, with effective hopping activation energy  $E_a$  varying between 0.12 eV at 125 K and 0.16 eV at 220 K, and most probable hopping range varying between 100 and 125% of the decay length of the localized polaron's wavefunction. Above 215 K a new contribution appears in the conductivity, accompanied by a weak endothermic feature in the calorimetric thermogram, which might signal a solid-solid phase transition. A broad dielectric loss feature is observed in the imaginary part of the permittivity. Such feature stems largely from a conductivity-related frequency-dependent loss associated with polaron hopping, as confirmed by the validity of the Barton-Nakajima-Namikawa condition.

**KEYWORDS:** Fullerene derivatives; organic molecular solid; universal dielectric response; dielectric spectroscopy; variable range hopping; relaxation loss.<sup>†</sup>



GRAPHICAL ABSTRACT

\* Corresponding Author. Phone: 34-934016568. E-mail: roberto.macovez@upc.edu.

<sup>†</sup> ABBREVIATIONS. DSC, differential scanning calorimetry; TGA, thermogravimetry analysis; VRH, variable-range hopping; BNN, Barton-Nakajima-Namikawa.

## 1. Introduction

Fullerenes, the fourth known allotrope of carbon after diamond, graphite and amorphous carbon, display intriguing conduction and molecular dynamic properties.<sup>1,2</sup> Thanks to their relatively high electron affinity, fullerenes and their derivatives usually behave as electron-transporting (*n*-channel) materials and as such they have been successfully implemented in electrical and optoelectronic devices such as high-efficiency fullerene-polymer-blend heterojunction solar cells,<sup>3,4</sup> high-mobility vacuum C<sub>60</sub> field-effect transistors,<sup>5</sup> and air-stable *n*-channel organic transistors.<sup>6,7</sup> Understanding the charge transport properties of fullerene-based systems is of crucial importance for the design of novel carbon materials with improved performance. Most small-molecule organic materials such as fullerenes behave as disordered inorganic semiconductors, where the main conduction mechanism is by polaronic (electron or hole) hopping.<sup>8</sup> The hopping-mediated conductivity is a consequence of strong local interactions that tend to localize charge carriers, such as inter-electron Coulomb repulsion and polarization screening,<sup>9</sup> coupling to molecular vibrations,<sup>10</sup> or trapping at defects.

Due to their globular shape, C<sub>60</sub> and some of its derivatives display rotational motions and orientational phase transformations in the solid state. For example, solid C<sub>60</sub> displays a face-centered cubic (*fcc*) rotator phase of freely spinning molecules at room temperature, while below 260 K the free-rotor motion is reduced to a ratcheting motion between two preferred orientations.<sup>11,12</sup> This merohedral reorientational motion finally freezes out at a glass transition taking place at 90 K, below which the lattice structure is simple cubic with four non-equivalent orientations.<sup>13,14,15</sup> Similar transitions are observed at very similar temperatures in simple derivatives such as C<sub>60</sub>O and the annulene isomer of C<sub>61</sub>H<sub>2</sub>,<sup>16,17</sup> albeit in the room-temperature *fcc* phase of the latter compounds the molecules do not behave as free rotors due to the fact that the adducts must occupy interstitial voids in-between the fullerene moieties. The cyclopropane isomer of C<sub>61</sub>H<sub>2</sub> displays instead a different phase diagram than its annulene isomer, exhibiting in particular an orientational melting occurring through a two-step transition around 198–213 K.<sup>18</sup>

In pristine C<sub>60</sub>, orientational ordering strongly favors electronic charge transport: across the transition at 260 K, the dc conductivity of C<sub>60</sub> raises by more than one order of magnitude,<sup>19</sup> and a similar behavior was observed in C<sub>60</sub> salts across the *fcc* to simple cubic transition.<sup>1</sup> This would indicate that molecular reorientations in crystalline fullerenes hinder electron hopping, possibly because they favor coupling to intermolecular vibrations and because the disorder induced by molecular reorientational motions leads to even stronger electron localization on single fullerene molecules and yet smaller electronic bandwidth.<sup>9</sup> Less is known on the effect of molecular motions in fullerene derivatives or polycrystalline and disordered fullerene systems.

Dielectric spectroscopy, closely related to impedance spectroscopy, is a versatile technique that allows studying in a single experiment both the conduction properties and the molecular dynamics of a sample.<sup>20</sup> In this contribution we employ dielectric spectroscopy to investigate electrical conduction and dipolar molecular dynamics in the solid phase of the halofullerene C<sub>60</sub>Br<sub>6</sub> derivative. We show that the conductivity below 215 K is due to hopping-mediated electronic charge transport, and provide values of the hopping energy and typical hopping range. Above 215 K a new conduction mechanism sets in, whose onset is marked by a weak endothermic peak in the calorimetric thermogram. The new conductivity contribution may thus be triggered or accompanied by the onset of a molecular motion. In the radiofrequency region, the material exhibits a conductivity-related dielectric loss analogous to that observed<sup>21,22</sup> in another fullerene derivative (C<sub>60</sub>(ONa)<sub>24</sub>) and typical of disordered or inhomogeneous

conductors,<sup>23,24</sup> which is ascribed to the accumulation of polaronic charge carriers at spatial inhomogeneity of the sample such as grain boundaries.

## 2. Experimental

For the preparation of C<sub>60</sub>Br<sub>6</sub> a procedure based on Troshin et al.<sup>25</sup> was followed. In a typical synthesis, 79 mg of pristine fullerene (C<sub>60</sub>, Aldrich, 99.8% pure) were dissolved in a mixture of 2 mL of elementary bromine and 10 mL of carbon disulfide. The resulting mixture was allowed to stand without stirring and heating for 10 days. The precipitate was filtered off, washed with hexane and dried at room temperature. The as-synthesized powder was characterized by thermogravimetric analysis (TGA) and scanning calorimetry (DSC). TGA curves were acquired while heating the sample under N<sub>2</sub> flow between room temperature (300 K) and 450 K by means of a Q50 thermobalance from TA-Instruments. DSC measurements were carried out between 200 K and 450 K using a Q100 calorimeter from TA-Instruments. In both experiments the heating rate was set to 10 K min<sup>-1</sup>, and the powder was placed in an open vessel to allow evaporation of volatile species.

For broadband dielectric spectroscopy measurements, the powder was mechanically pressed into pellets of submillimeter thickness between 7 mm-diameter stainless steel electrode disks in parallel-plate capacitor geometry. Dielectric spectra were acquired in the frequency range from 10<sup>-2</sup> to 10<sup>7</sup> Hz using a Novocontrol Alpha analyzer. Isothermal frequency scans were acquired between 125 and 360 K (with a temperature stability of ±0.3 K) in a N<sub>2</sub> flow Quatro cryostat (the sample was in a nitrogen flux during all measurements). Dielectric spectroscopy yields the complex conductivity and permittivity of a sample as a function of frequency ( $f$ ) of the applied ac electric voltage. The  $\sigma'(f)$  spectra (real part of the ac conductivity) display a plateau value at low frequency, corresponding to the dc value of the conductivity,  $\sigma_{dc}$ . In order to study the temperature dependence of  $\sigma_{dc}$ , an effective activation energy of the conductivity (slope of the tangent to the curve of  $\text{Ln}(\sigma_{dc})$  versus  $k_B T$ ) is computed as

$$(1) E_a(\sigma_{dc}) = -\frac{d(\text{Ln}(\sigma_{dc}))}{d(1/k_B T)}.$$

The imaginary part of the permittivity  $\varepsilon''(f)$ , called loss spectrum, is related to the real part of the ac conductivity  $\sigma'(f)$  as  $\varepsilon''(f) = \sigma'(f)/(2\pi f \varepsilon_0)$ . The loss spectrum contains information about the characteristic frequency of dielectric losses such as molecular reorientational motions, and about conductivity-induced losses. Each ac conductivity spectrum and corresponding loss spectrum were fitted as the sum of one or more relaxation processes, modeled with the Havriliak-Negami function, on top of a background representing the dc conductivity contribution. The analytic expression of the Havriliak–Negami function is:<sup>26,27</sup>

$$(2) \varepsilon_{HN}(f) = \varepsilon_\infty + \frac{\Delta\varepsilon}{(1+(i2\pi f \tau_{HN})^\beta)^\gamma}.$$

Here  $\Delta\varepsilon = \varepsilon_s - \varepsilon_\infty$  is the dielectric strength,  $\varepsilon_\infty$  and  $\varepsilon_s$  being the high-frequency and static low-frequency limits of the real permittivity. The parameters  $\beta$  and  $\gamma$ , which lie in the range from 0 to 1, are related with the shape and asymmetry of the relaxation time distribution; finally,  $\tau_{HN}$  is a fitting parameter from which the characteristic time  $\tau$  at which the dielectric loss of the given relaxation process is maximum is obtained as:

$$(3) \tau = \tau_{HN} \left( \sin \frac{\beta\pi}{2+2\gamma} \right)^{-1/\beta} \left( \sin \frac{\beta\gamma\pi}{2+2\gamma} \right)^{1/\beta}.$$

### 3. Results and Discussion

Figure 1(a) shows a typical TGA curve of the as-synthesized powder, both as mass percent and as its first derivative. The main mass loss observed at about 390 K corresponds to slightly above 35% in weight, which is in agreement with the expected mass decrease upon loss of all bromine atoms in  $C_{60}Br_6$  (the theoretical value is  $479.4/1200.1 = 40\%$ ). The recovered product after heating to 450 K is polycrystalline  $C_{60}$ , as determined from powder X-ray diffraction experiments (not shown). At lower temperature, a smaller mass loss is observed in the range between room temperature and 340 K due to volatile impurities, likely  $Br_2$  or carbon disulfide, both of which are employed in the synthesis (see Experimental Section). Molecules of bromine and/or of organic solvents are known to remain trapped in the solid matrix during the synthesis process of brominated fullerenes and  $C_{60}Br_6$  in particular, sometimes even leading to the formation of solvates.<sup>25,28,29</sup> As visible in Figure 1(b), the DSC thermogram exhibits two endothermic peaks in correspondence with each mass loss.

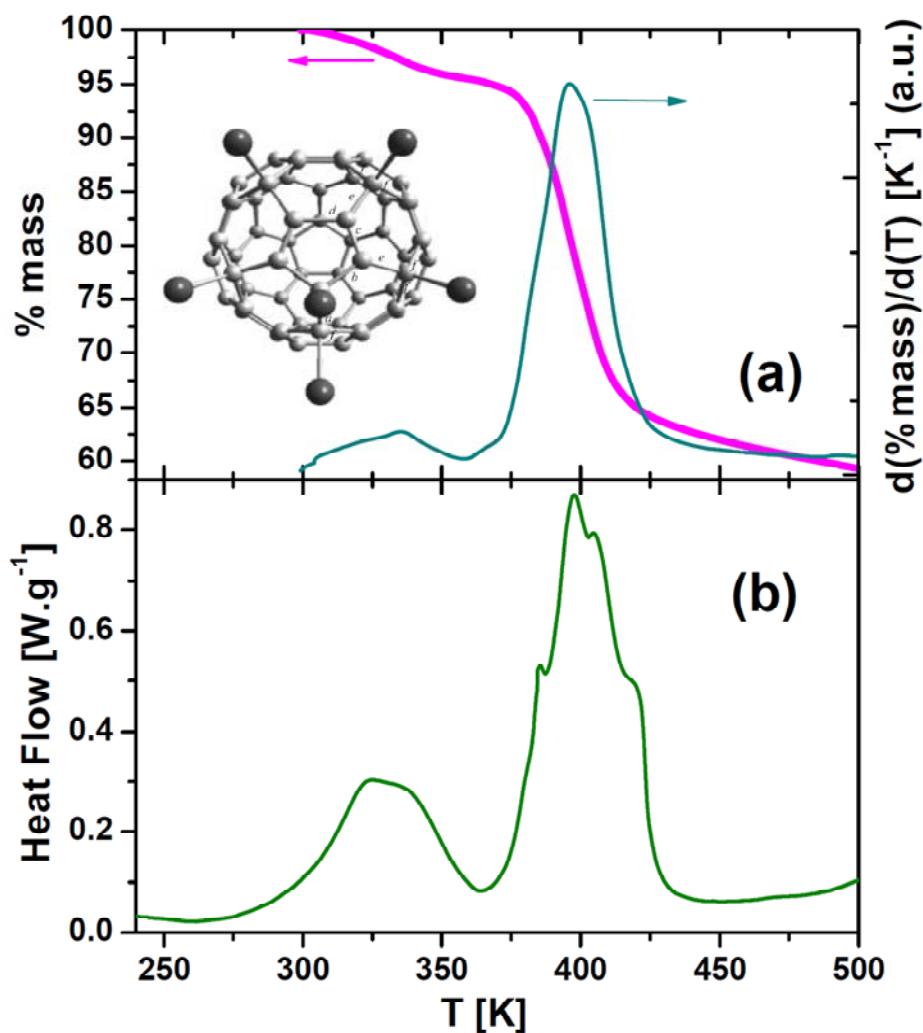


**Fig. 1.** TGA (a) and DSC (b) curves measured on the as-synthesized  $C_{60}Br_6$  powder upon heating. In (a), the thin line is the first derivative of the percent mass loss (thick line), and the molecular structure of  $C_{60}Br_6$  is shown as inset.

In light of these results, for the characterization of  $C_{60}Br_6$  by means of dielectric spectroscopy the powder was pre-heated to 323 K prior to acquisition of the spectra, in order to remove all volatile impurities present in the powder<sup>30</sup> (heating to 343 K did not further modify the spectral response). Figure 2 shows the frequency-dependent ac conductivity spectra (a) and loss spectra (b) of a typical (pre-heated)  $C_{60}Br_6$  pellet, as measured upon heating from 125 K. Similar data were obtained by measuring while subsequently cooling the sample from room temperature. The lineshape of the ac conductivity spectra  $\sigma'(f)$  is similar to that of a very wide range of disordered systems ranging from amorphous semiconductors and glasses to metal-cluster compounds to polymers and polymer composites. In all these materials the conductivity is frequency-independent at low frequencies, reaching a plateau value corresponding to the dc value ( $\sigma_{dc}$ ), and then, above a temperature-dependent onset frequency, exhibits a power-law-like dependence on  $f$ , described approximately by:

$$(4) \sigma'(f) = \sigma_{dc} + \sigma_0 f^s.$$

Eq. (4) is known as the universal ac dielectric response.<sup>21,23,24,31,32,33,34</sup> In the case of  $C_{60}Br_6$ , the universal ac conduction law gives an only rough fit to the experimental spectra, which in logarithmic scale exhibit a curved rather than linear lineshape for frequencies above the onset of the ac response. A fit of the spectra with Eq. (4) gives values of the exponent  $s$  in the range of 0.6-0.7, which is consistent with hopping of localized (polaronic) states.<sup>35</sup> The only approximate validity of the universal Eq. (4) is due to the presence of a dielectric loss, which is clearly visible in Figure 2(b) as a broad bump-like feature above the low-temperature linear dc-conductivity background. Many disordered conductors have similar ac conductivity spectra, in which the separation between the dc and ac regimes of the conductivity is signaled by a dielectric loss in the radiofrequency range.<sup>23</sup> In most cases such loss is associated with charge accumulation due to spatial inhomogeneities of the dc conductivity.<sup>36</sup> The detailed origin of the loss feature in the case of  $C_{60}Br_6$  is discussed later.

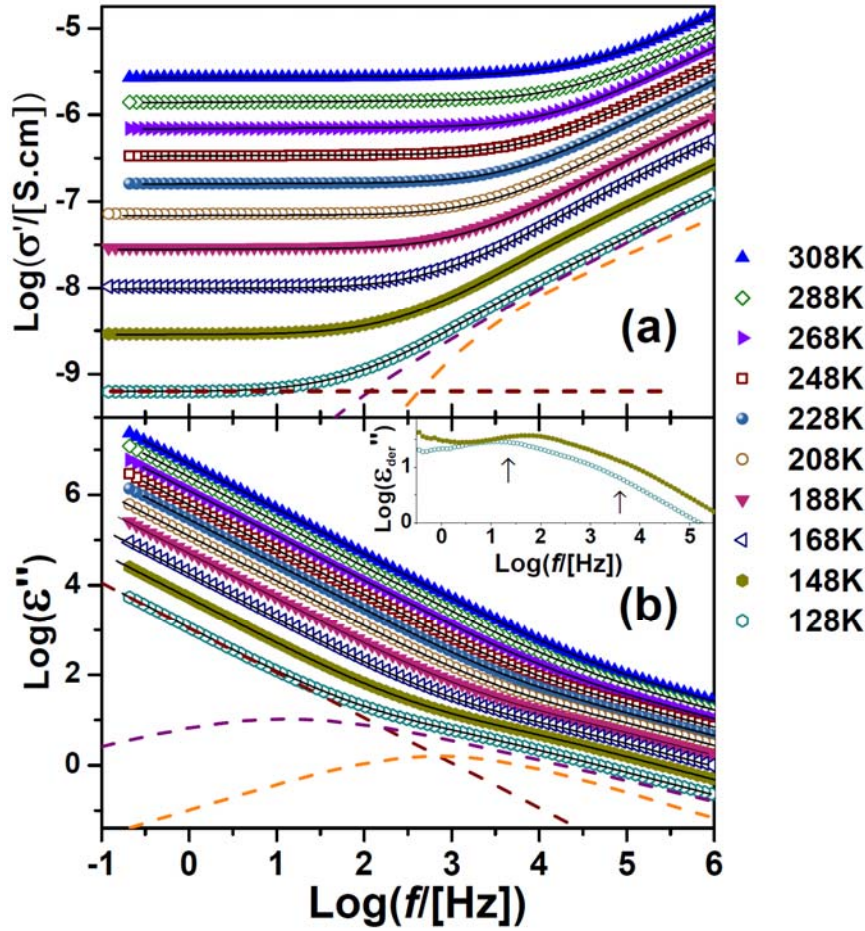


**Fig. 2.** Logarithmic plot of the ac conductivity  $\sigma'$  (a) and dielectric loss  $\epsilon''$  (b) spectra of  $C_{60}Br_6$ , shown for selected temperatures (between 308 and 128 K, every 20 K). Continuous lines are fits with Havriliak-Negami components on top of a background representing the dc conductivity limit. The fit components are shown as dashed lines for the spectrum acquired at 128 K. Inset to (b): logarithmic derivative spectrum  $\epsilon''_{der}$  shown for two selected temperatures (128 and 148 K; see the text for the definition). The arrows indicate the position of the two components present in the spectrum.

Fig. 3(a) depicts the Arrhenius plot of the dc conductivity ( $\sigma_{dc}$ ), extracted directly as the plateau value in the  $\sigma'$  spectra of Fig. 2(b). It may be observed that  $\sigma_{dc}$  does not exhibit a simply activated (Arrhenius) behavior, but rather displays a negative curvature in the whole probed temperature range (125-330 K). To study the temperature dependence of the conductivity in more detail, we have calculated the effective (temperature-dependent) activation energy  $E_a$  of the dc conductivity using Eq. (1), and represented this quantity as a function of temperature in the logarithmic plot shown in Fig. 3(b). Although the effective activation energy is a monotonic function of temperature (always increasing with increasing temperature), it may be observed that it exhibits markedly different temperature dependences above and below approximately 215 K. The logarithmic plot of Fig. 3(b) clearly highlights the existence of two conduction regimes, one characterized by a slope of  $0.49 \pm 0.02$  and the other with a slope of  $1.36 \pm 0.02$  in the logarithmic representation. It is interesting to notice that a small endothermic feature is detected at the same temperature in the DSC thermogram, as shown in the inset to Figure 3(b). The onset of the new conduction mechanism therefore accompanies a fundamental change in the material.

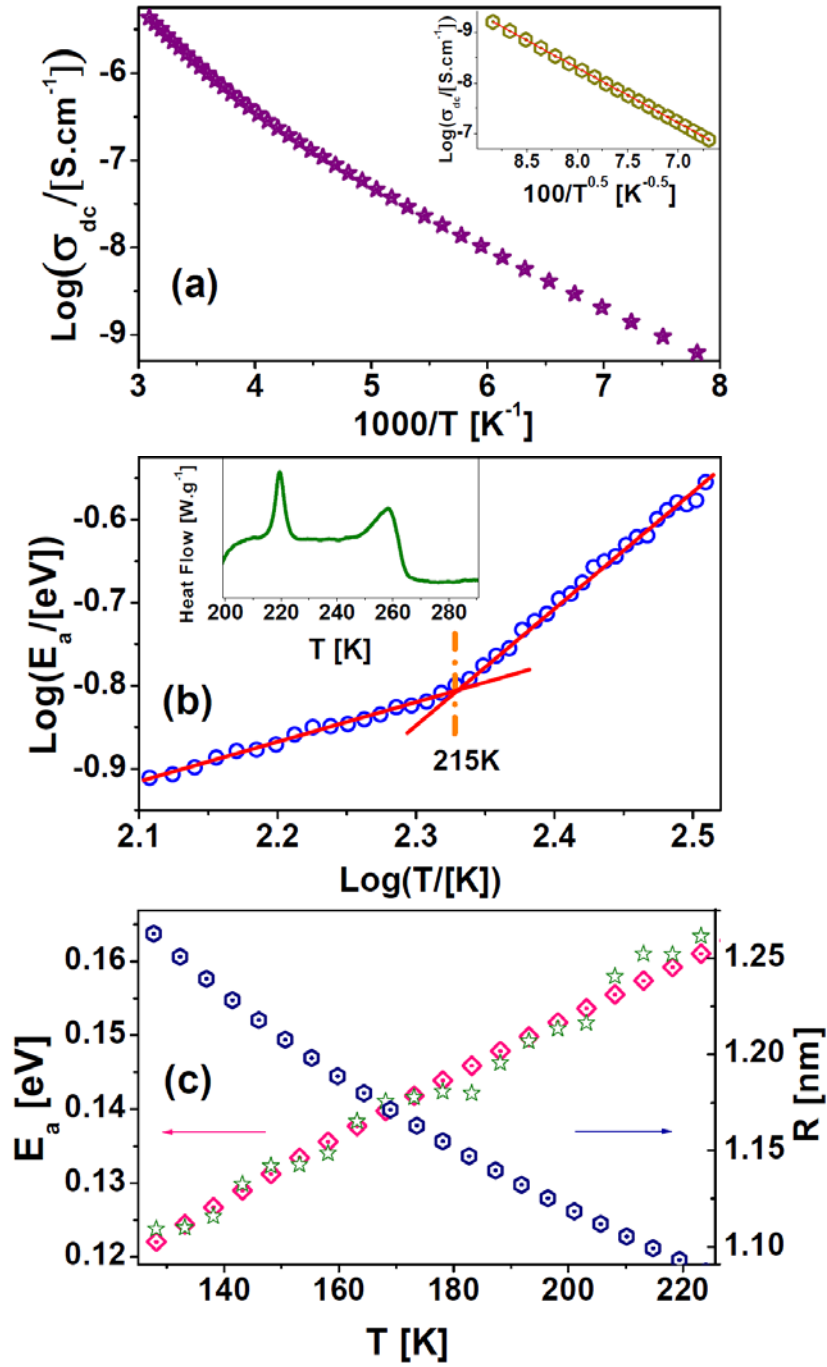


**Fig. 3.** (a) Semilogarithmic plot of the dc conductivity  $\sigma_{dc}$  of  $C_{60}Br_6$  vs  $1000/T$  (Arrhenius plot) between 125 and 330 K. Inset: plot of  $\text{Log}(\sigma_{dc})$  vs  $100/\sqrt{T}$  below 220 K, for the same data as in the main panel. (b) Logarithmic plot of the activation energy  $E_a$  (in eV) of the dc conductivity, vs temperature. The continuous lines are linear fits of the data below and above 215 K, respectively. The dashed vertical line indicates the cross-over temperature between the two regimes, as determined by the intersection of both linear fits. Inset: DSC scan acquired on the same sample upon heating from 200 K. (c) Activation energy  $E_a$  and hopping distance  $R$  as a function of temperature for VRH conduction in  $C_{60}Br_6$  below 220 K. Stars are experimental points obtained using Eq. (1) and dotted squares are calculated values by means of Eq. (7) (see the text for more details).

The data below 215 K are consistent with an electronic charge transport described by Mott's variable range hopping (VRH) model.<sup>37</sup> According to this model, the logarithm of the dc conductivity should follow a fractional power-law dependence, given by:

$$(5) \sigma_{dc} = \sigma_0 \exp[-(T_0/T)^p].$$

Here  $\sigma_0$  and  $T_0$  are constants and the exponent  $p$  is usually equal to 1/2 or 1/4. Applying the definition of activation energy (Eq. (1)) to Eq. (5), one finds that the slope of the logarithmic plot of  $E_a$  vs  $T$  plot should be equal to  $1 - p$ .<sup>35</sup> The slope of  $0.49 \pm 0.02$  obtained below 215 K gives a value of  $p$  of  $0.51 \pm 0.02$ , which is virtually identical to the theoretical value of 1/2 of the VRH model, observed in many systems characterized by hopping electronic conduction, ranging from metal-cluster compounds to granular and ceramic metals, to doped or amorphous organic and inorganic semiconductors.<sup>21,31,32,34,38,39</sup> The value  $p = 1/2$  is determined by electron-electron correlation<sup>32</sup> leading to a weak Coulomb gap near the Fermi level<sup>34</sup> and to a square dependence of the localized state density on energy.<sup>40,41</sup> The inset to Fig. 3(a) shows the logarithmic plot of  $\sigma_{dc}$  vs  $1/T^{0.5}$  below 220 K to highlight the consistency with the VRH model. Fig. 3(c) shows the activation energy  $E_a$  and typical hopping distance  $R$  in the same temperature range. The typical hopping distance is given by:<sup>35</sup>

$$(6) R = \xi (T_0/192T)^{0.25}.$$

Here  $\xi$  is the decay length of the localized electronic wavefunction, and  $T_0 = 6.25 \pm 0.05 \cdot 10^4$  K is the temperature parameter in Eq. 5, as determined from the fit of the  $\sigma_{dc}$  values below 215 K. From Eq. (6) it is found that the value of  $R$  decreases from  $1.27\xi$  to  $1.08\xi$  as the temperature is raised from 125 to 225 K. Fig. 3(c) shows a plot of the hopping distance  $R$  assuming that  $\xi = 1$  nm, *i.e.* equal to the van der Waals radius of the  $C_{60}$  molecule.<sup>42</sup> The activation energy shown as a function of temperature in the same plot was calculated both using Eq. (1) and according to the formula:

$$(7) E_a = 0.5k_B T_0^{0.5} T^{0.5}$$

which is valid for the case of VRH with  $p = 0.5$ . As visible from the figure, Eq. (7) gives values consistent with those obtained directly from the raw data using Eq. (1).

The results discussed so far show that charge conduction in  $C_{60}Br_6$  has a dominant contribution below 215 K due to variable-range hopping of localized electronic states (or holes), as expected from the known electron affinity and  $n$ -channel behavior of  $C_{60}$  derivatives.<sup>2</sup> The value of the slope of the  $\text{Log}(E_a)$  vs  $\text{Log}(T)$  plot above 215 K is inconsistent with the variable-range hopping model, as such theory predicts a slope between zero and one (a slope close to zero would correspond to a simply-activated Arrhenius behavior). However, the fact that the activation energy increases with increasing temperature suggests that the conduction is still electronic in nature above 215 K, since the opposite behavior (decrease of  $E_a$  with increasing temperature) is usually observed in the case of ionic conduction.<sup>20,43</sup> On the other hand, the fact that a new dominant charge conduction mechanism starts being effective only above the threshold temperature of 215 K is reminiscent of the behavior of another fullerene derivative, namely the polymeric salt  $Li_4C_{60}$ .<sup>44,45</sup> In this material, the conductivity above 130 K is dominated by the contribution of  $Li^+$  ions,<sup>46</sup> which become mobile only above this temperature.<sup>47</sup> A possible ion-conduction mechanism in  $C_{60}Br_6$  could be associated with the diffusion of ionic impurities or, less likely, to the intermolecular exchange of  $Br^-$  ions.

The precise nature of the transition at 215 K is at present unclear. The shape of the DSC feature in the inset to Figure 3(b) as well as the lack of a clear relaxation feature in the spectra of Figure 2 above this

temperature (see below) indicate that it is not an orientational glass transition as the one of pure  $C_{60}$  at 90 K,<sup>13,14,15</sup> but rather it might be a solid-solid transition between phases with different orientational order. The associated enthalpy of transition is  $0.5\pm 0.2$  J/gr or  $600\pm 250$  kJ/mol, which indicates that the degree of molecular order might be similar in both the phases above and below 215 K. Since we do not observe any new dielectric relaxation at 215 K, if an orientational transition takes place in  $C_{60}Br_6$  then either both phases are crystalline, with no orientational dynamics. This is also consistent with the higher conductivity in the high-temperature phase, as rotational melting should lead to lower conductivity as in pristine  $C_{60}$ .<sup>19</sup> It is seen in the inset to Figure 3(b) that a second, rather broad, endothermic feature is present at higher temperature, between 250 and 260 K. It might be that the solid-solid phase transition is not a single-step transition. Such behavior is for example observed for the orientational phase transition in the solid phase of the cyclopropane isomer of  $C_{61}H_2$ , which as mentioned in the Introduction occurs in two steps between 198 and 125 K.<sup>18</sup>

We finally discuss the dielectric losses in the material. Albeit the  $C_{60}Br_6$  molecules possess a non-zero permanent dipole moment, given that solid  $C_{60}Br_6$  is a crystalline material<sup>25</sup> we do not expect to observe dipolar relaxations (especially below 215 K). A different possible origin for the wide radiofrequency feature visible at low temperature in the isothermal  $\varepsilon''(f)$  spectra of Fig. 2(b) might be a conductivity-induced relaxation, *i.e.*, a loss feature associated with the accumulation of (free) electronic charge carriers at spatial inhomogeneities of the sample such as grain boundaries. A loss feature of this kind was for example reported in another fullerene derivative,  $C_{60}(NaO)_{24}$ .<sup>21</sup>

A quantitative fitting analysis was carried out to corroborate this assignment in  $C_{60}Br_6$ . We found that the loss feature on Fig. 2(b) could not be fitted with a single Havriliak-Negami (HN) function (Eq. (2)), but actually contained two contributions. The presence of two loss features may be best observed in the logarithmic derivative of the imaginary permittivity, defined as  $\varepsilon''_{der} = -\frac{\pi}{2} \frac{\partial \varepsilon''(\omega)}{\partial \ln(\omega)}$ , where  $\omega = 2\pi f$  and  $\varepsilon'$  is the real part of the permittivity (which is measured simultaneously with the imaginary part). The logarithmic derivative is a good approximation to the dielectric loss without the ohmic-conduction contribution, and can be employed to better visualize ac losses.<sup>48</sup>

The logarithmic derivative spectra are shown in the inset to Fig. 2(b) for two temperatures (128 and 148 K). It may be seen that the ohmic-conduction-free loss indeed contains two contributions, whose spectral positions are indicated by arrows, both of which shift to higher frequency with increasing temperature as expected. Each dielectric spectrum (both in the ac conductivity and permittivity representations) was therefore fitted as the sum of a background proportional to reciprocal frequency (dc conductivity) and the imaginary part of two HN functions representing distinct loss features. The obtained fits are displayed as continuous lines in Figure 2. The fit components are shown explicitly for the spectrum acquired at the lowest temperature displayed in both representations (128 K).

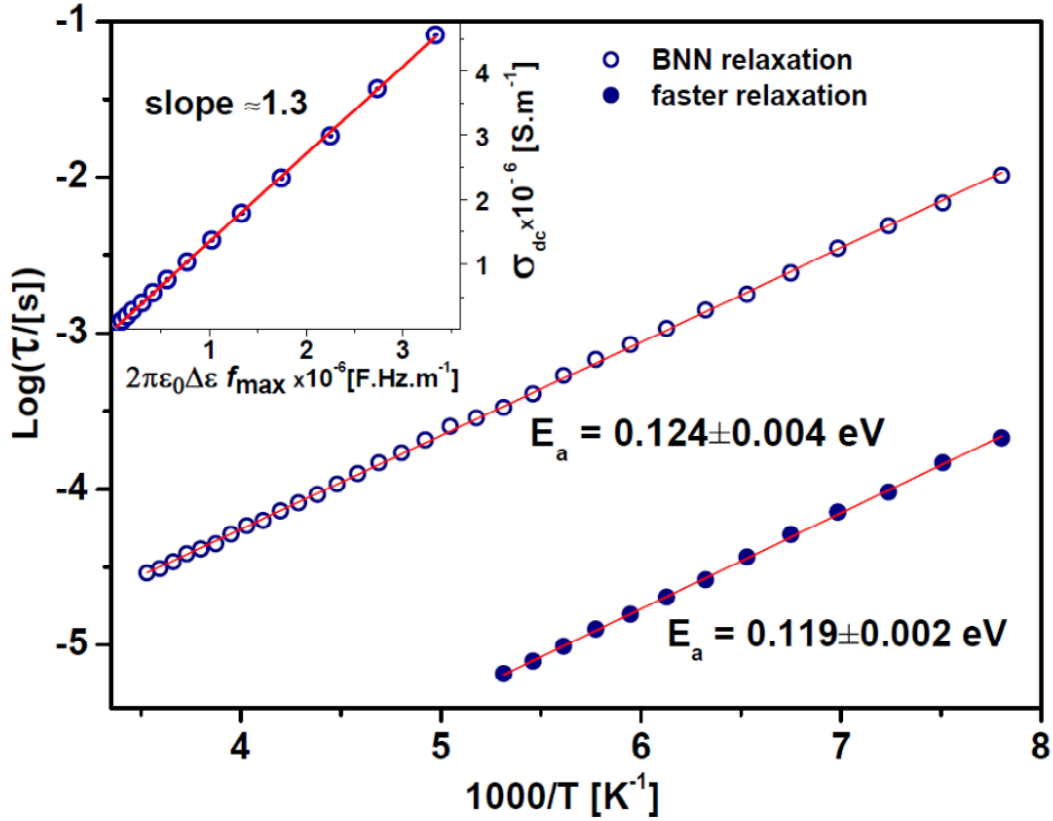


**Fig. 4.** Arrhenius plot of the characteristic times  $\tau$  of both dielectric loss features in  $C_{60}Br_6$  (markers), and corresponding Arrhenius fits (continuous lines). Inset: plot of  $\sigma_{dc}$  versus the quantity  $2\pi\epsilon_0\Delta\epsilon/\tau$  calculated for the most prominent dielectric loss. The continuous line is a linear fit to verify the validity of the BNN relationship below 230 K (see the text).

Fig. 4 shows the temperature dependence of the relaxation times  $\tau$  of the two loss peaks in  $C_{60}Br_6$ . Both relaxations roughly follow an Arrhenius behavior, with similar slopes. The inset to Fig. 4 is a plot, for temperatures below 230 K, of the dc conductivity  $\sigma_{dc}$  as a function of the quantity  $2\pi\epsilon_0\Delta\epsilon/\tau$  calculated for the slower and most prominent dielectric loss, *i.e.*, the one with longer relaxation times ( $\Delta\epsilon$  is the dielectric strength and  $\tau$  is the relaxation time, see Eq. 2). It is seen that both quantities are linearly correlated (with a slope of 1.3) in the temperature range where the conductivity is electronic in character ( $T < 230$  K). This correlation, known as Barton-Nakajima-Namikawa relationship,<sup>49</sup> is typical of the conductivity-induced loss observed in many samples at the onset of the ac regime of the conductivity. This result shows that the most prominent (slower) component in the loss spectrum is indeed a conductivity-related loss associated to the hopping of polaronic species.<sup>21,32</sup> Above 230 K, the validity of the BNN relation breaks down, with the plot depicted in the inset to Fig. 4 exhibiting a sub-linear dependence. This is a consequence of the onset of the new conduction mechanism and the breakdown of the VRH theory.

As to the faster relaxation feature, it might be dipolar in character or else share the same conductivity-related origin as the slower one. The slopes of the Arrhenius plot (activation energies) of both relaxations are quite similar, which could suggest a similar origin. For example, the two features could stem from inhomogeneities on two different length scales, one associated with grain boundaries (as it is

common for a space-charge relaxation), and another with the molecular scale, associated with polarization effects due to electron confinement on single molecules, as recently proposed for  $C_{60}(ONa)_{24}$ .<sup>21</sup> Another option is that the faster relaxation is dipolar in nature. If one extrapolates its Arrhenius dependence to lower temperature, a freezing temperature of 70 K is obtained for this faster process (following the usual convention for glass-forming materials, the freezing temperature is defined as the temperature at which the relaxation time equals 100 s, *i.e.*,  $\text{Log}(\tau) = 2$ ). This value actually represent a lower limit for the actual freezing temperatures, as we cannot exclude a Vogel-Fulchert-Tamman temperature dependence of the relaxation time especially close to freezing. It may therefore be concluded that the freezing temperature of the fast dynamic process in  $C_{60}Br_6$  is close to the glass transition temperature of pure  $C_{60}$  (90 K)<sup>11,12,13,14,15</sup> and of the  $C_{60}O$  derivative (100 K).<sup>17</sup> A dipolar relaxation might be displayed by labile  $C_{60}Br_6$  moieties at grain boundaries or in amorphous regions of the sample, if present.

#### 4. Conclusions

We have analyzed the conduction and dielectric properties of the fullerene derivative  $C_{60}Br_6$  by means of temperature-dependent dielectric spectroscopy. Electrical conduction below 220 K is due to hopping processes of electronic charge carriers and it is well described by Mott's variable-range hopping (VRH) model, while above this temperature a new conduction mechanism, likely also electronic in character, sets in. The effective average activation energy for electronic hopping increases with temperature, from 0.12 at 125 K to 0.16 eV at 220 K. The imaginary permittivity spectra display two loss features. The lower-frequency and more prominent of the two features obeys the Barton-Nakajima-Namikawa relation, which shows that the main dipolar loss in  $C_{60}Br_6$  is a space-charge-like dielectric loss accompanying the hopping of polaronic charge carriers, in agreement with expectations for a crystalline phase.

#### Acknowledgments

This work has been partially supported by the Spanish Ministry of Science and Innovation MINECO through project FIS2014-54734-P and by the Generalitat de Catalunya under project 2014 SGR-581.

#### References

---

<sup>1</sup> Macovez, R.; Goldoni, A.; Petaccia, L.; Brühwiler, P.A.; Rudolf, P. Reversible Phase Transformation and Doubly Charged Anions at the Surface of Simple Cubic  $RbC_{60}$ . *Phys. Rev. Lett.* **2008**, *101*, 236403.

<sup>2</sup> Mitsari, E.; Romanini, M.; Zachariah, M.; Macovez, R. Solid State Physicochemical Properties and Applications of Organic and Metallo-Organic Fullerene Derivatives. *Curr. Org. Chem.* **2016**, *20*, 645-661.

<sup>3</sup> He, Z.; Zhong, C.; Su, S.; Xu, M.; Wu, H.; Cao, Y. Enhanced Power-Conversion Efficiency in Polymer Solar Cells Using an Inverted Device Structure. *Nat. Photonics* **2012**, *6*, 591-595.

<sup>4</sup> Lai, Y.-Y.; Cheng, Y.-J.; Hsu, C.-S. Applications of Functional Fullerene Materials in Polymer Solar Cells. *Energy Environ. Sci.* **2014**, *7*, 1866-1883.

<sup>5</sup> Anthopoulos, T.D.; Singh, B.; Marjanovic, N.; Sariciftci, N.S.; Ramil, A.M.; Sitter, H.; Cölle, M.; de Leeuw, D.M. High Performance N-channel Organic Field-Effect Transistors and Ring Oscillators based on  $C_{60}$  Fullerene Films. *Appl. Phys. Lett.* **2006**, *89*, 213504.

- 
- <sup>6</sup> Jones, B. A.; Facchetti, A.; Wasielewski, M. R.; Marks, T. J. Tuning Orbital Energetics in Arylene Diimide Semiconductors. Materials Design for Ambient Stability of N-Type Charge Transport. *J. Am. Chem. Soc.* **2007**, *129*, 15259–15278
- <sup>7</sup> Usta, H.; Risko, C.; Wang, Z.; Huang, H.; Delimeroglu, M. K.; Zhukovitskiy, A.; Facchetti, A.; Marks, T. J. Design, Synthesis, and Characterization of Ladder-Type Molecules and Polymers. Air-Stable, Solution-Processable N-Channel and Ambipolar Semiconductors for Thin-Film Transistors via Experiment and Theory. *J. Am. Chem. Soc.* **2009**, *131*, 5586–5608
- <sup>8</sup> Brutting, W.; Adachi, Ch. (Ed.s). *Physics of Organic Semiconductors*, 2<sup>nd</sup> Ed. Wiley (**2012**)
- <sup>9</sup> Macovez, R.; Hunt, M. R. C.; Goldoni, A.; Pedio, M.; Rudolf, P. Surface Hubbard U of Alkali Fullerides. *J. Electron Spectr. Relat. Phenom.* **2011**, *183*, 94–100
- <sup>10</sup> Gunnarsson, O. Superconductivity in Fullerides. *Rev. Mod. Phys.* **1997**, *69*, 575-606
- <sup>11</sup> Tycko, R.; Dabbagh, G.; Fleming, R.M.; Haddon, R.C.; Makhija, A.V.; Zahurak, S.M. Molecular Dynamics and the Phase Transition in Solid C<sub>60</sub>. *Phys. Rev. Lett.* **1991**, *67*, 1886.
- <sup>12</sup> David, W.I.F.; Ibberson, R.M.; Matthewman, J.C.; Prassides, K.; Dennis, T.J.; Hare, J.P.; Kroto, H.W.; Taylor, R.; Walton, D.R.M. Crystal Structure and Bonding of Ordered C<sub>60</sub>. *Nature* **1991**, *353*, 147–149
- <sup>13</sup> Gugenberger, F.; Heid, R.; Meingast, C.; Adelman, P.; Braun, M.; Wühl, H.; Haluska, M.; Kuzmany, H. Glass Transition in Single-Crystal C<sub>60</sub> Studied by High-Resolution Dilatometry. *Phys Rev Lett.* **1992**, *69*, 3774.
- <sup>14</sup> Heiney, P.A.; Fischer, J. E.; McGhie, A.R.; Romanow, W.J.; Denenstein, A.M.; Jr. McCauley, J.P.; Smith, A.B.; Cox, D.E. Orientational Ordering Transition in Solid C<sub>60</sub>. *Phys. Rev. Lett.* **1991**, *66*, 2911.
- <sup>15</sup> Dworkin, A.; Szwarc, H.; Leach, S.; Hare, J.P.; Dennis, T.J.; Kroto, H.W.; Taylor, R.; Walton, D.R.M. Thermodynamic evidence for a phase transition in crystalline fullerene C<sub>60</sub>. *C. R. Acad. Sci. II* **1991**, *312*, 979–982
- <sup>16</sup> Lommen, A.N.; Heiney, P.A.; Vaughan, G.B.M.; Stephens, P.W.; Liu, D.; Li, D.; Smith, A.L.; McGhie, A.R.; Strongin, R.M.; Brard, L.; Smith III, A.B. Structure and Phase Transition of the 6,5-Annulene Isomer of C<sub>61</sub>H<sub>2</sub>. *Phys. Rev. B* **1994**, *49*, 12572.
- <sup>17</sup> Meingast, C.; Roth, G.; Pintschovius, L.; Michel, R.H.; Stoermer, C.; Kappes, M.M.; Heiney, P.A.; Brard, L.; Strongin, R.M.; Smith III, A.B. Structure, Dynamics, and Phase Transitions in the Fullerene Derivatives C<sub>60</sub>O and C<sub>61</sub>H<sub>2</sub>. *Phys. Rev. B* **1996**, *54*, 124.
- <sup>18</sup> Stetzer, M.R.; Heiney, P.A.; Stephens, P.W.; Dinnebier, R. E.; Zhu, Q.; McGhie, A.R.; Strongin, R.M.; Brandt, B.M.; Smith III, A.B. Structure and Phase Transitions of the 6,6-Cyclopropane Isomer of C<sub>61</sub>H<sub>2</sub>. *Phys. Rev. B* **2000**, *62*, 9305.
- <sup>19</sup> Katz, E. A.; Faiman, D.; Iakoubovskii, K.; Isakina, A.; Yagotintsev, K. A.; Strzhemechny, M. A.; Balberg, I. Effect of the Disorder/Order Phase Transition on the Electrical and Photoelectrical Properties of C<sub>60</sub> Thin Films. *J. Appl. Phys.* **2003**, *93*, 3401
- <sup>20</sup> Zachariah, M.; Romanini, M.; Tripathi, P.; Tamarit, J.Ll.; Macovez, R. Molecular Diffusion and Dc Conductivity Perfectly Correlated with Molecular Rotational Dynamics in a Plastic Crystalline Electrolyte. *Phys. Chem. Chem. Phys.* **2015**, *17*, 16053–16057.

- 
- <sup>21</sup> Macovez, R.; Zachariah, M.; Romanini, M.; Zygouri, P.; Gournis, D.; Tamarit, J.Ll. Hopping Conductivity and Polarization Effects in a Fullerene Derivative Salt. *J. Phys. Chem. C* **2014**, *118*, 12170–12175.
- <sup>22</sup> Zachariah, M.; Mitsari, E.; Romanini, M.; Zygouri, P.; Gournis, D.; Barrio, M.D.; Tamarit, J.Ll.; Macovez, R. Water-Triggered Conduction Mediated by Proton Exchange in a hygroscopic Fulleride and its Hydrate. *J. Phys. Chem. C* **2015**, *119*, 685–694
- <sup>23</sup> Jonscher, A. K. The ‘Universal’ Dielectric Response. *Nature* **1977**, *267*, 673.
- <sup>24</sup> Dyre, J. C.; Schroder, T. B. Universality of Ac Conduction in Disordered Solids. *Rev. Mod. Phys.* **2000**, *72*, 873-892
- <sup>25</sup> Troshin, P. A.; Kemnitz, E.; Troyanov, S. I. Characterization of Reactions of Fullerene C<sub>60</sub> with Bromine. Crystal structures of Bromofullerenes C<sub>60</sub>Br<sub>6</sub>, C<sub>60</sub>Br<sub>6</sub>•CS<sub>2</sub>, C<sub>60</sub>Br<sub>8</sub>•CHBr<sub>3</sub>•2Br<sub>2</sub>, and C<sub>60</sub>Br<sub>24</sub>•C<sub>6</sub>H<sub>4</sub>Cl<sub>2</sub>•Br<sub>2</sub>. *Russian Chemical Bulletin, International Edition* **2004**, *53*, 2787 –2792
- <sup>26</sup> Havriliak S.; Negami, S. A complex Plane Analysis of  $\alpha$ -Dispersions in Some Polymer Systems. *J. Polym. Sci.-Pt. C* **1966**, *16*, 99–117.
- <sup>27</sup> Havriliak S.; Negami, S. A complex Plane Representation of Dielectric and Mechanical Relaxation Processes in Some Polymers. *Polymer* **1967**, *8*, 161–210.
- <sup>28</sup> Birkett, P.R.; Hitchcock, P.B.; Kroto, H.W.; Taylor, R.; Walton, D.R.M. Preparation and characterization of C<sub>60</sub>Br<sub>6</sub> and C<sub>60</sub>Br<sub>8</sub>. *Nature* **1992**, *357*, 479-481
- <sup>29</sup> Birkett, P.R.; Crane, J.D.; Hitchcock, P.B.; Kroto, H.W.; Meidine, M.F.; Taylor, R.; Walton, D.R.M. The structural characterization of buckminsterfullerene compounds. *J. Mol. Struct.* **1993**, *292*, 1.
- <sup>30</sup> Macovez, R.; Mitsari, E.; Zachariah, M.; Romanini, M.; Zygouri, P.; Gournis, D.; Tamarit, J. Ll. Ultraslow Dynamics of Water in Organic Molecular Solids. *J. Phys. Chem. C* **2014**, *118*, 4941–4950.
- <sup>31</sup> van Staveren, M. P. J.; Brom, H. B.; de Jongh, L. J. Metal-Cluster Compounds and Universal Features of the Hopping Conductivity of Solids. *Phys. Rep.* **1991**, *208*, 1-96
- <sup>32</sup> Capaccioli, S.; Lucchesi, M.; Rolla, P. A.; Ruggeri, G. Dielectric Response Analysis of a Conducting Polymer Dominated by the Hopping Charge Transport. *J. Phys.: Condens. Matter.* **1998**, *10*, 5595–5617
- <sup>33</sup> Lunkenheimer, P.; Lloid, A. Response of Disordered Matter to Electromagnetic Fields. *Phys. Rev. Lett.* **2003**, *91*, 207601
- <sup>34</sup> Huijbregts, L. J.; Brom, H. B.; Brokken-Zijp, J. C. M.; Kemerink, M.; Chen, Z.; de Goeje, M. P.; Yuan, M.; Michels, M. A. J. The Optimal Structure-Conductivity Relation in Epoxy-Phthalocyanine Nanocomposites. *J. Phys. Chem. B* **2006**, *110*, 23115-23122
- <sup>35</sup> Han, H.; Davis, C.; Nino, J.C. Variable Range Hopping Conduction in BaTiO<sub>3</sub> Ceramics Exhibiting Colossal Permittivity. *J. Phys. Chem. C* **2014**, *118*, 9137–9142
- <sup>36</sup> Yamamoto K.; Namikawa, H. Conduction Current Relaxation of Inhomogeneous Conductor I. *Jpn. J. Appl. Phys. Part 1* **1988**, *27*, 1845
- <sup>37</sup> Mott, N. F.; Davis, E. A. *Electronic Processes in Noncrystalline Materials* (Clarendon, Oxford, **1979**).

- 
- <sup>38</sup> Tran, T. B.; Beloborodov, I. S.; Lin, X. M.; Bigioni, T. P.; Vinokur, V. M.; Jaeger, H. M. Multiple Cotunneling in Large Quantum Dot Arrays. *Phys. Rev. Lett.* **2005**, *95*, 076806
- <sup>39</sup> Yu, D.; Wang, C.; Wehrenberg, B. L.; Guyot-Sionnest, P. Variable Range Hopping Conduction in Semiconductor Nanocrystal Solids. *Phys. Rev. Lett.* **2004**, *92*, 216802
- <sup>40</sup> Efros, A.L.; Shklovskii, B.I. Coulomb Gap and Low Temperature Conductivity of Disordered Systems. *J. Phys. C: Solid State Phys.* **1975**, *8*, L49–L51
- <sup>41</sup> Shklovskii, B. I.; Efros, A. L. Electronic Properties of Doped Semiconductors. Springer: Berlin (1984).
- <sup>42</sup> Saito, S.; Oshiyama, A. Cohesive Mechanism and Energy Bands Of Solid C<sub>60</sub>. *Phys. Rev. Lett.* **1991**, *66*, 2637-2640.
- <sup>43</sup> Zachariah, M.; Romanini, M.; Tripathi, P.; Barrio, M.; Tamarit, J.Ll.; Macovez, R. Self-diffusion, phase behavior, and Li<sup>+</sup> ion conduction in succinonitrile-based plastic co-crystals. *J. Phys. Chem. C* **2015**, *119*, 27298–27306.
- <sup>44</sup> Margadonna, S.; Pontiroli, D.; Belli, M.; Shiroka, T.; Riccò, M.; Brunelli, M. Li<sub>4</sub>C<sub>60</sub>: A Polymeric Fulleride with a Two-Dimensional Architecture and Mixed Interfullerene Bonding Motifs. *J. Am. Chem. Soc.* **2004**, *126*, 15032–15033
- <sup>45</sup> Riccò, M.; Shiroka, T.; Belli, M.; Pontiroli, D.; Pagliari, M.; Ruani, G.; Palles, D.; Margadonna, S.; Tomaselli, M. Unusual Polymerization in the Li<sub>4</sub>C<sub>60</sub> Fulleride. *Phys. Rev. B* **2005**, *72*, 155437
- <sup>46</sup> Macovez, R.; Savage, R.; Venema, L.; Schiessling, J.; Kamaras, K.; Rudolf, P. Low Band Gap and Ionic Bonding with Charge Transfer Threshold in the Polymeric Lithium Fulleride Li<sub>4</sub>C<sub>60</sub>. *J. Chem. Phys. C* **2008**, *112*, 2988–2996
- <sup>47</sup> Riccò, M.; Belli, M.; Mazzani, M.; Pontiroli, D.; Quintavalle, D.; Janossy, A.; Csanyi, G. Superionic Conductivity in the Li<sub>4</sub>C<sub>60</sub> Fulleride Polymer. *Phys. Rev. Lett.* **2009**, *102*, 145901
- <sup>48</sup> Wübbenhorst, M.; van Turnhout, J. Analysis of Complex Dielectric Spectr. I. One-Dimensional Derivative Techniques and Three-Dimensional Modelling. *J. Non-Cryst. Solids* **2002**, *305*, 40–49
- <sup>49</sup> Namikawa, H. Characterization of the Diffusion Process in Oxide Glasses Based on the Correlation between Electric Conduction and Dielectric Relaxation. *J. Non-Cryst. Solids* **1975**, *18*, 173